The Astrophysical Journal, 718:913–919, 2010 August 1 doi:10.1088/0004-637X/718/2/913

GRAVITATIONAL LENSING CORRECTIONS IN FLAT ΛCDM COSMOLOGY

Ronald Kantowski[1], Bin Chen[1], and Xinyu Dai[1,2]
[1] Homer L. Dodge Department of Physics and Astronomy, University of Oklahoma, Norman, OK 73019, USA; kantowski@nhn.ou.edu, Bin.Chen-1@ou.edu, dai@nhn.ou.edu
[2] Department of Astronomy, University of Michigan, Ann Arbor, MI 48109, USA
Received 2009 September 16; accepted 2010 June 7; published 2010 July 7

ABSTRACT

We compute the deflection angle to order $(m/r_0)^2$ and $m/r_0 \times \Lambda r_0^2$ for a light ray traveling in a flat ΛCDM cosmology that encounters a completely condensed mass region. We use a Swiss cheese model for the inhomogeneities and find that the most significant correction to the Einstein angle occurs not because of the nonlinear terms but instead occurs because the condensed mass is embedded in a background cosmology. The Swiss cheese model predicts a decrease in the deflection angle of ∼2% for weakly lensed galaxies behind the rich cluster A1689 and that the reduction can be as large as ∼5% for similar rich clusters at $z \approx 1$. Weak-lensing deflection angles caused by galaxies can likewise be reduced by as much as ∼4%. We show that the lowest order correction in which Λ appears is proportional to $m/r_0 \times \sqrt{\Lambda r_0^2}$ and could cause as much as a ∼0.02% increase in the deflection angle for light that passes through a rich cluster. The lowest order nonlinear correction in the mass is proportional to $m/r_0 \times \sqrt{m/r_0}$ and can increase the deflection angle by ∼0.005% for weak lensing by galaxies.

Key words: cosmology: theory – gravitational lensing: strong – gravitational lensing: weak

Online-only material: color figure

1. INTRODUCTION

Recently, Rindler & Ishak (2007) have stirred interest in the possibility of measuring the cosmological constant Λ through its effect on the deflection of light that traverses large galaxy clusters by asserting that Λ has a non-negligible effect on small angle bending. Several papers have since appeared to support the existence of an effect (Ishak 2008; Ishak et al. 2008, 2010; Sereno 2008, 2009; Schücker 2009a), although qualitatively disagreeing on its value and/or interpretation, but others (Park 2008; Khriplovich & Pomeransky 2008) contest the existence of an effect arguing that the additional bending caused by Λ vanishes when measured by observers moving with the Hubble flow. We purport to give the definitive answer to this question as well as several other related ones. When comparing observations with and without a Λ, one must compare observations of two different sets of events, by two different observers, in two different universes. One ideally attempts to make common as many kinematic and dynamic properties as possible in the two gedanken experiments. To conclude whether Λ does or does not cause bending can easily depend on what is held in common and what property is compared in the two experiments. For example, a photon orbit in a Kottler (1918) spacetime (Schwarzschild with a cosmological constant) does not depend on Λ if static coordinates are used, see Equations (3) and (11). One could hence conclude that Λ does not affect bending. However, as Rindler & Ishak (2007) point out, observers, stationary relative to the Schwarzschild mass, will measure an angle between the photon direction and the radial direction that does depend on Λ. From this observation, one could conclude that Λ does affect bending. Both conclusions are valid, but neither answers the outstanding question, "how does Λ contribute to deflections caused by large inhomogeneities in the otherwise homogeneous background cosmology?" This is just one of the questions we definitively answer, subject to the condition that the inhomogeneity is significantly condensed and has no peculiar motion.

To correctly analyze Λ's nonlinear effect on bending, we found it necessary to use exact solutions to Einstein's equations. These solutions reveal a somewhat surprising value for the lowest order nonlinear correction in the deflecting mass m to the familiar Einstein deflection formula $4Gm/c^2r_0$ (see the square root term in Equation (32)). This correction, like the Λ correction, increases the deflection and occurs because the deflector is embedded in a universe that expands. By using an exact inhomogeneous cosmology, the largest correction to $4Gm/c^2r_0$ is revealed not to be a nonlinear term but instead is caused by the limited time the deflector has to influence a passing photon (see the $\cos^3\tilde{\phi}_1$ term in Equations (32) and (33)). The limited time or equivalently the limited range of the inhomogeneity can be thought of as a result of shielding by the homogeneous background in which the deflecting mass is embedded and decreases the deflection (relative to the Einstein value). General relativity (GR) requires that the two gravity fields, the homogeneous background and the local inhomogeneity, be appropriately matched at their bounding surface. We use the Swiss cheese models because they are the only known exact GR solutions that embed spherical inhomogeneities in expanding homogeneous universes. Gravitational lensing calculations in cosmology are usually done by superimposing a deflecting mass on top of a homogeneous mass density and ignoring any boundary matching. The resulting deflection angle is obtained by a simple summation of the Einstein expression $4Gm/c^2r_0$. The results can at best be accurate to first order in the ratio of mass m to minimum impact distance r_0, and if the shielding predicted by boundary matching in Swiss cheese is accurate, the linear term can be in error by a few percent in physically realizable circumstances (see Figure 4).

Because our goal is to correctly present the higher order corrections and because a simple superposition of the masses is not satisfactory, we resort to using exact solutions to Einstein's gravity (see Section 2). It is in the nonlinear corrections that the cosmological constant first appears. What we calculate in this paper is (in a series approximation) the angle $\alpha \equiv \xi_2 - \xi_1$

(see Figure 1) between two spatial directions ξ_2 and ξ_1 as seen by comoving observers in a flat Robertson–Walker (RW) spacetime, where ξ_1 is the spatial direction of a photon before it encounters an inhomogeneity here described by the vacuum Kottler spacetime (see Equation (3)) and ξ_2 is the direction of the photon after it has emerged from the Kottler condensation. The dynamics of the RW metric is determined by GR sourced by pressure-free matter (often referred to as dust) and includes a cosmological constant. These are relatively simple Friedman–Lemaître–Robertson–Walker (FLRW) cosmological models, see Equation (1). Because the RW cosmology used is spatially flat and non-rotating, (1) the angle between any two comoving spatial directions is well defined independently of when or where the directions are measured and (2) the spatial direction of an undeflected photon remains fixed.

In Section 2, we describe the inhomogeneous cosmology we use and in Section 3 we outline some details of how we compute the bending angle of a photon that encounters an inhomogeneity. In Section 4, we discuss limits on the usefulness of our results and compare the Einstein angle with our corrected results for deflections caused by inhomogeneities ranging from galaxies to rich clusters.

2. SWISS CHEESE: LOCALLY INHOMOGENEOUS COSMOLOGIES

We use a single condensation in a Swiss cheese cosmology to compute light deflections caused by local inhomogeneities so there can be no doubt about errors introduced by gravity approximations. Because Swiss cheese is an exact solution to Einstein's equations (Einstein & Straus 1945; Schücking 1954), its use ensures the accuracy of the superposed gravity field and automatically takes into account the finite range of the mass density perturbation as well as observer aberration. The model was first used by Kantowski (1969a) without the cosmological constant to settle the dispute as to whether or not inhomogeneities affected mean luminosities. At that time, the validity of predictions (Zel'dovich 1964; Dashevskii & Zel'dovich 1965; Dashevskii & Slysh 1966; Bertotti 1966; Gunn 1967) obtained using approximate GR solutions, which indicated that mass concentrations caused the average distance–redshift relation to differ from the pure homogeneous value, were being questioned. Even though the results are occasionally doubted by some, the Swiss cheese model gave the definitive answer—there is an effect (see Kantowski et al. 1995). This model again comes to the rescue by clearly demonstrating the extent to which the cosmological constant Λ influences the small angle bending of a photon that passes a single mass concentration (see Equation (32)). Even though others have computed bending angles that depended on Λ, until now, questions abound as to their usefulness and/or accuracy in a cosmological setting. We have succeeded in giving a rigorously derived expression for this deflection.

The Swiss cheese model simultaneously accounts for the finite size of the deflector's influence, the motion of the cosmic observers, and the nonlinear effects of gravity. The basic idea of Swiss cheese is to remove non-overlapping comoving spheres of homogeneous dust from one of the homogeneous FLRW cosmologies and replace them with gravity fields representing appropriately condensed spherical mass distributions. If the cosmology is without a cosmological constant, the simplest replacements are Schwarzschild metrics and if there is a Λ, the simplest replacements are Kottler metrics (Dyer & Roeder 1974). These condensations are the most extreme for Swiss cheese. An infinite number of less extreme models can be constructed by using the Lemaître–Tolman–Bondi metrics (Lemaître 1933; Tolman 1934; Bondi 1947) to represent spherically symmetric dust concentrations (Kantowski 1969b). In all Swiss cheese models, the metric that is used to fill a dust condensation must match first and second fundamental forms on the boundary. In the case of Schwarzschild, the metric's mass is fixed by the dust's density and the size of the condensed hole, and in the case of Kottler, Λ is additionally required to be the same inside as it is outside. In this calculation, we stick with the extreme but unique condensation, the Kottler metric, to arrive at a unique deflection angle. Schücker (2009b) uses this same model but because he only considers a single numerical example, his results are difficult to compare with ours.

The two metrics are: outside, flat ($\Omega_\Lambda + \Omega_m = 1$) FLRW

$$ds^2 = -c^2 dT^2 + R(T)^2[d\chi^2 + \chi^2(d\theta^2 + \sin^2\theta\, d\phi^2)], \quad (1)$$

with the cosmic time development given by the Friedman equation

$$\frac{\dot{R}}{R} = H_0\sqrt{\Omega_\Lambda + \Omega_m\left(\frac{R_0}{R}\right)^3}, \quad (2)$$

and inside, the static Kottler metric (Kottler 1918)

$$ds^2 = -\gamma(r)^{-2}c^2dt^2 + \gamma(r)^2dr^2 + r^2(d\theta^2 + \sin^2\theta\, d\phi^2), \quad (3)$$

where $\gamma(r)$ is defined by

$$\gamma(r) \equiv 1\Big/\sqrt{1 - \frac{r_s}{r} - \frac{\Lambda r^2}{3}}. \quad (4)$$

Boundary matching at comoving FLRW radius χ_b constrains the Schwarzschild radius r_s of the condensed mass to be

$$r_s = \Omega_m \frac{H_0^2}{c^2}(R_0\chi_b)^3, \quad (5)$$

and the additional Kottler parameter Λ to coincide with the FLRW value, i.e.,

$$\Lambda = 3\Omega_\Lambda \frac{H_0^2}{c^2}. \quad (6)$$

The Kottler and RW angular coordinates are matched at the boundary and the radius of the Kottler hole expands according to

$$r_b(T) = R(T)\chi_b \quad (7)$$

(for some numerical examples, see the mass and r_b columns of Table 1). As seen by a stationary Kottler observer, the dust boundary of the Kottler hole moves with Lorentz parameters β_b and γ_b given by

$$\gamma_b \equiv \gamma(r_b),$$
$$\beta_b \equiv \sqrt{1 - \gamma_b^{-2}} = H_b r_b/c, \quad (8)$$

where H_b is the time-dependent Hubble parameter of the boundary. The normalized 4-velocity of the boundary coincides with the RW comoving dust velocity $\hat{u}_{\rm RW}$ at the boundary and is of the form

$$\hat{u}_{\rm RW} = \gamma_b\,\hat{u}_K + \beta_b\gamma_b\,\hat{r}_K, \quad (9)$$

when expressed in terms of unit Kottler time and radial vectors, respectively, $\hat{u}_K$ and $\hat{r}_K$.

Table 1
Examples of Gravitational Lensing Corrections in ΛCDM Cosmology

Name	Lensing	Redshift	Mass ($M_\odot$)	r_b (Mpc)	Impact Angle (arcsec)	$\tilde{\phi}_1$ (deg)	$1-\cos^3\tilde{\phi}_1$	Ratio1[a]	Ratio2[b]
A1689	Strong	0.18	8×10^{13}	6.6	45	1.2	0.00065	2.2×10^{-6}	1.4
A1689	Weak	0.18	10^{15}	15.3	600	6.8	0.021	0.00017	1.4
RDCS 1252−2927	Weak	1.24	10^{15}	8.0	180	11	0.052	0.00040	0.20
Elliptical galaxy	Strong	0.5	3×10^{11}	0.8	2	0.87	0.00035	1.7×10^{-7}	0.69
Elliptical galaxy	Weak	0.5	10^{13}	2.6	70	9.6	0.041	6.6×10^{-5}	0.69

Notes.

[a] Ratio1 $\equiv 4\tan\tilde{\phi}_1\sqrt{\frac{\Lambda r_0^2}{3}+\frac{r_s}{r_0}\sin^3\tilde{\phi}_1}$ (the ratio of the next order correction to the lowest order term, see Equation (32)).

[b] Ratio2 $\equiv \frac{\frac{\Lambda r_0^2}{3}}{\frac{r_s}{r_0}\sin^3\tilde{\phi}_1}$ (measures the relative importance of Λ in the square root term).

3. THE PHOTON'S PATH

In Figure 1, we show the spatial orbit of a slightly deflected photon $r(\phi)$ that enters and exits a Kottler condensation. The coordinates have been rotated to put the orbit in the $\theta=\pi/2$ plane and to make it symmetric about $\phi=\pi/2$ while in Kottler. The tangent to the photon's geodesic path is

$$k=\frac{\ell}{r_0}\left[\frac{\gamma(r)}{\gamma_0}\hat{u}_K\pm\sqrt{\frac{\gamma(r)^2}{\gamma_0^2}-\frac{r_0^2}{r^2}}\,\hat{r}_K-\frac{r_0}{r}\hat{\phi}_K\right], \tag{10}$$

where ℓ is an angular momentum like constant; r_0 is the minimum r and occurs at $\phi=\pi/2$; $\gamma_0\equiv\gamma(r_0)$; and $\hat{u}_K$, $\hat{r}_K$, and $\hat{\phi}_K$ are unit vectors pointing respectively in the static time, radial, and azimuthal Kottler directions. The actual orbit $r(\phi)$ is approximated as

$$\begin{aligned} r/r_0=\csc\phi\Bigg\{&1-\left(\frac{r_s}{2r_0}\right)[-1+2\csc\phi-\sin\phi]+\left(\frac{r_s}{2r_0}\right)^2\\ &\times\left[-\frac{17}{4}+\frac{15}{4}\left(\phi-\frac{\pi}{2}\right)\cot\phi+4\csc^2\phi+\frac{1}{4}\sin^2\phi\right]\Bigg\}\\ &+\mathcal{O}\left[\left(\frac{r_s}{2r_0}\right)^3\right]. \end{aligned} \tag{11}$$

For this to be a valid expansion, not only must $r_s/r_0\ll1$ but ϕ must also satisfy $\sin\phi\gg r_s/r_0$. The tangent to the photon as it travels in the $\theta=\pi/2$ plane of a flat RW spacetime is of the form

$$k=\frac{\mathrm{con}}{R(T)}[\hat{u}_{\mathrm{RW}}+\cos(\phi-\xi)\hat{\chi}-\sin(\phi-\xi)\hat{\phi}_{\mathrm{RW}}], \tag{12}$$

where $\hat{u}_{\mathrm{RW}}$, $\hat{\chi}$, and $\hat{\phi}_{\mathrm{RW}}$ are respectively unit comoving time, radial, and azimuthal vectors in RW. The significance of the constant angle ξ is that $\tan\xi$ is the slope of the photon's straight line orbit in the comoving x–y plane (see Figure 1). When the photon's tangent vector is matched across the boundary of the dust hole, the following single (exact) constraint results

$$[1+\beta_b\cos(\phi_b-\xi)]\frac{r_0}{r_b}=\frac{\sin(\phi_b-\xi)}{\gamma_0}, \tag{13}$$

where r_b, ϕ_b, and β_b are evaluated at the photon's entrance/exit point on the boundary of the Kottler hole. From Equation (13), we obtain the following exact expression for ξ

$$\begin{aligned} \sin\xi=&\left\{-B\frac{r_0}{r_b}\pm A\sqrt{1-\left(\frac{r_0}{r_b}\right)^2-\frac{r_s}{r_0}\left[1-\left(\frac{r_0}{r_b}\right)^3\right]}\right\}\Bigg/\\ &\left\{1-\frac{r_s}{r_0}\left[1-\left(\frac{r_0}{r_b}\right)^3\right]\right\}, \end{aligned} \tag{14}$$

where

$$\begin{aligned} A&\equiv\cos\phi_b\,\beta_b\frac{r_0}{r_b}-\frac{\sin\phi_b}{\gamma_0},\\ B&\equiv\sin\phi_b\,\beta_b\frac{r_0}{r_b}+\frac{\cos\phi_b}{\gamma_0}. \end{aligned} \tag{15}$$

The $-A$ choice is made in Equation (14) at the exit point and the Kottler coordinates on the boundary are taken as $r_b=r_2$, $\phi_b=\phi_2$. The $+A$ choice is made at the entrance point and the Kottler coordinates are taken as $r_b=r_1$, $\phi_b=\pi-\tilde{\phi}_1$, ($\tilde{\phi}_1$ is the supplement of the entrance azimuthal coordinate; see Figure 1).

In what follows we give some of the details necessary to approximately evaluate the deflection angle $\alpha=\xi_2-\xi_1$ caused by encountering a condensation in the homogeneous dust. The reader not interested in the details can jump to the result called α_{total} given in Equation (32). The calculation is somewhat complicated because the Kottler hole expands as it is traversed by the photon. The deflection angle naturally divides into a part that depends on the initial size of the hole (α_{static} given in Equation (23)) and an additional part caused by the extended path required of the photon to exit the expanded hole (α_{expand} given in Equation (31)). The extended path, described by Δr and $\Delta\phi$, is given in Equations (28) and (30) (see Figure 1). We will see that the expansion part gives the most significant nonlinear part of the correction to the familiar Einstein term $4Gm/c^2r_0$.

3.1. Approximation Details

To compute the photon's direction ξ in the dust approximately, we assume that both Λr_0^2 and r_s/r_0 are small (perhaps even of the same order) and expand Equation (14) in the two small parameters:

$$\delta\equiv\sqrt{\frac{\Lambda r_0^2}{3}+\frac{r_s}{r_0}\left(\frac{r_0}{r_b}\right)^3}=\beta_b\frac{r_0}{r_b}, \tag{16}$$

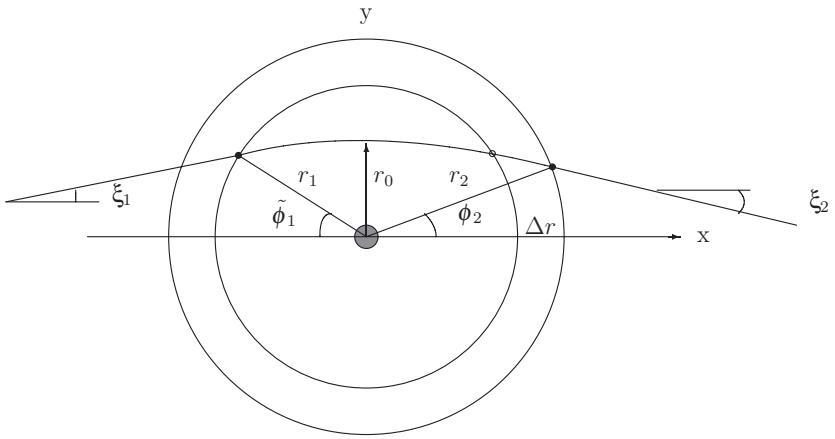

Figure 1. Photon travels from left to right entering a Kottler hole at $r = r_1,\ \phi = \pi - \tilde{\phi}_1$ and returns to the FLRW dust at $r = r_2,\ \phi = \phi_2$. The photon's orbit has been chosen to be symmetric in Kottler about the point of the closest approach $r = r_0,\ \phi = \pi/2$. Due to the cosmological expansion, $\Delta r \equiv r_2 - r_1 > 0$. The slope of the photon's comoving trajectory in the x–y plane is ξ_1 when incoming and ξ_2 after exiting. The resulting deflection angle as seen by comoving observers in the FLRW background is $\alpha = \xi_2 - \xi_1$.

and

$$\delta_m^2 \equiv \frac{r_s}{r_0}\left(\frac{r_0}{r_b}\right)^3. \tag{17}$$

The result is

$$\xi = -\delta + C_2(\phi_b)\delta_m^2 - \frac{1}{6}\delta^3 + C_3(\phi_b)\delta_m^2\delta + C_4(\phi_b)\delta_m^4 + \mathcal{O}(\delta^5), \tag{18}$$

where the coefficients are defined by

$$\begin{aligned} C_2(\phi_b) &\equiv -\cot\phi_b\left(\frac{1}{2} + \csc^2\phi_b\right), \\ C_3(\phi_b) &\equiv \frac{1}{2}(1 - \csc^3\phi_b), \\ C_4(\phi_b) &\equiv \csc^6\phi_b\left[\frac{15}{32}(2\phi_b - \pi) + \cot\phi_b\left(3 - \sin\phi_b\right.\right. \\ &\quad \left.\left. - \frac{15}{16}\sin^2\phi_b - \frac{1}{2}\sin^3\phi_b + \frac{1}{8}\sin^4\phi_b + \frac{1}{4}\sin^6\phi_b\right)\right]. \end{aligned} \tag{19}$$

From Equation (14), we can conclude that when $r_s \to 0$, $\sin\xi \to -\delta = -\sqrt{\Lambda r_0^2/3}$ exactly with no dependence on r_b or ϕ_b. This limit is consistent with Equation (18). The conclusion is that when $r_s = 0$ there is no Λ bending. This is an obvious conclusion because the spacetime inside and outside of the hole is exactly the same, i.e., no physical difference exists between the inside and the outside. The only difference is in which coordinates are being used.

When $0 < r_s \ll r_0$, we proceed by eliminating r_1 and r_2 using Equation (11) and then expanding ϕ_2 about $\tilde{\phi}_1$ by writing

$$\phi_2 = \tilde{\phi}_1 + \Delta\phi. \tag{20}$$

This gives us two terms to evaluate

$$\alpha_{\rm static} \equiv \xi_2(\tilde{\phi}_1) - \xi_1(\pi - \tilde{\phi}_1), \tag{21}$$

and

$$\alpha_{\rm expand} \equiv \left(\frac{d\xi}{d\phi}\right)_{\tilde{\phi}_1}\Delta\phi + \frac{1}{2}\left(\frac{d^2\xi}{d\phi^2}\right)_{\tilde{\phi}_1}(\Delta\phi)^2 + \frac{1}{6}\left(\frac{d^3\xi}{d\phi^3}\right)_{\tilde{\phi}_1} \times (\Delta\phi)^3 + \mathcal{O}(\Delta\phi)^4. \tag{22}$$

The first term can be evaluated immediately using Equations (18) and (19) giving the Λ independent expression:

$$\begin{aligned} \alpha_{\rm static} = &-2\left(\frac{r_s}{2r_0}\right)\cos\tilde{\phi}_1[2 + \sin^2\tilde{\phi}_1] + \left(\frac{r_s}{2r_0}\right)^2 \\ &\times\left[\frac{15}{4}(2\tilde{\phi}_1 - \pi) + \cos\tilde{\phi}_1\left(4 - \frac{15}{2}\sin\tilde{\phi}_1 + 2\sin^2\tilde{\phi}_1\right.\right. \\ &\left.\left. + 7\sin^3\tilde{\phi}_1 + 2\sin^5\tilde{\phi}_1\right)\right] + \mathcal{O}\left(\frac{r_s}{2r_0}\right)^3. \end{aligned} \tag{23}$$

By overlooking the expansion term, one would obviously conclude that there is no Λ bending. To evaluate $\alpha_{\rm expand}$, the expansion's contribution to bending requires that we compute $\Delta\phi$ (or equivalently Δr) caused by the expansion of the Kottler hole that took place during the time it took the photon to transit the hole. In Figure 2, we indicate how we compute Δr. We start by giving the entrance radius r_1 and look for the common solution to the boundary expansion $r_b(t)$ and the photon's radial coordinate $r_p(t)$; i.e., we put

$$c\int dt = c\int_{r_1}^{r_2}\left(\frac{dr_b}{dt}\right)^{-1}dr = c\int_{r_1}^{r_2}\left(\frac{dr_p}{dt}\right)^{-1}dr. \tag{24}$$

We rewrite the time it takes the photon to cross the hole as the sum of the time it takes to cross from r_1 on the left to r_1 on the right plus the extra time it takes to go from r_1 on the right to $r_2 = r_1 + \Delta r$. We then move this last time difference to the left-hand side and obtain the following equation to solve:

$$\begin{aligned} c\int_{r_1}^{r_2}\left[\left(\frac{dr_b}{dt}\right)^{-1} - \left(\frac{dr_p}{dt}\right)^{-1}\right]dr &= 2c\int_{r_0}^{r_1}\left(\frac{dr_p}{dt}\right)^{-1}dr \\ &= 2c\int_{\pi/2}^{\tilde{\phi}_1}\left(\frac{d\phi_p}{dt}\right)^{-1}d\phi. \end{aligned} \tag{25}$$

The right-hand side, RHS, is evaluated approximately using Equations (10) and (11) to obtain

$$\mathrm{RHS} = 2r_0\left\{\cot\tilde{\phi}_1 + \left(\frac{r_s}{2r_0}\right)\left[\cot\tilde{\phi}_1(1 - 2\csc\tilde{\phi}_1)\right.\right.$$

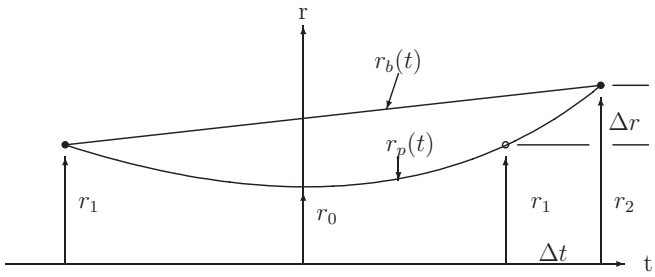

Figure 2. While a photon travels through a Kottler hole entering at $r = r_1$, $\phi = \pi - \tilde{\phi}_1$ and exiting at $r = r_2$, $\phi = \phi_2$, its radial coordinate varies with time as $r_p(t)$ and the boundary of Kottler hole continually expands according to $r_b(t)$. The exit coordinates differ from the entrance values by $\Delta\phi = \phi_2 - \tilde{\phi}_1$ and $\Delta r = r_2 - r_1$.

$$- 2\log\left(\tan\frac{\tilde{\phi}_1}{2}\right)\Bigg] + \frac{\Lambda r_0^2}{18}\cot\tilde{\phi}_1\left[1 + 2\csc^2\tilde{\phi}_1\right] + \mathcal{O}\left[\left(\frac{r_s}{2r_0}\right) + \Lambda r_0^2\right]^2\Bigg\}. \quad (26)$$

We call the two terms on the left-hand side of Equation (25) LHS_b and LHS_p and evaluate LHS_b by expanding in Δr,

$$\mathrm{LHS}_b = \left(\frac{\gamma_b^2}{\beta_b}\right)_{r_1}(\Delta r) + \frac{1}{2}\frac{d}{dr_b}\left(\frac{\gamma_b^2}{\beta_b}\right)_{r_1} \times (\Delta r)^2 + \frac{1}{6}\frac{d^2}{dr_b^2}\left(\frac{\gamma_b^2}{\beta_b}\right)_{r_1}(\Delta r)^3 + \mathcal{O}(\Delta r)^4, \quad (27)$$

where β_b and γ_b as functions of r_b are defined in Equation (8). Equation (11) can be used to convert Δr into $\Delta\phi$ resulting in

$$\Delta r = r_0\Bigg\{-\cos\tilde{\phi}_1\csc^2\tilde{\phi}_1\left[1 + \left(\frac{r_s}{2r_0}\right)(1 - 4\csc\tilde{\phi}_1) + \mathcal{O}\left(\frac{r_s}{2r_0}\right)^2\right]\Delta\phi + \frac{1}{2}\left[\csc^3\tilde{\phi}_1(2 - \sin^2\tilde{\phi}_1) + \mathcal{O}\left(\frac{r_s}{2r_0}\right)\right] \times (\Delta\phi)^2 + \frac{1}{6}\left[\cot\tilde{\phi}_1\csc\tilde{\phi}_1(1 - 6\csc^2\tilde{\phi}_1) + \mathcal{O}\left(\frac{r_s}{2r_0}\right)\right] \times (\Delta\phi)^3 + \mathcal{O}(\Delta\phi)^4\Bigg\}. \quad (28)$$

The second term on the left-hand side of Equation (25) can be evaluated by using $\phi_p(t)$ from Equation (10) rather than $r_p(t)$ (just as was done with RHS) and gives

$$\mathrm{LHS}_p = r_0\csc^2\tilde{\phi}_1\left\{\left[1 + \mathcal{O}\left(\frac{r_s}{r_0} + \Lambda r_0^2\right)\right](\Delta\phi) - \cot\tilde{\phi}_1\left[1 + \mathcal{O}\left(\frac{r_s}{r_0} + \Lambda r_0^2\right)\right](\Delta\phi)^2 + \mathcal{O}(\Delta\phi)^3\right\}. \quad (29)$$

3.2. The Resulting Deflection

Combining Equations (26), (27), and (29) in Equation (25), we obtain the change that occurs in the exiting value of ϕ; i.e., $\Delta\phi \equiv \phi_2 - \tilde{\phi}_1$, caused by the expansion of the hole's boundary as the photon traverses,

$$\Delta\phi = -2\beta_1\sin\tilde{\phi}_1 + \left(\frac{r_s}{r_0}\right)\Bigg[3\cos\tilde{\phi}_1\sin^2\tilde{\phi}_1 - \beta_1\left(2 + \frac{7}{3}\sin^2\tilde{\phi}_1 - 6\sin^4\tilde{\phi}_1 - 2\log\left\{\tan\frac{\tilde{\phi}_1}{2}\right\} \times \tan\tilde{\phi}_1\sin\tilde{\phi}_1\right)\Bigg] - \frac{1}{9}\beta_1\Lambda r_0^2\sin\tilde{\phi}_1 + \mathcal{O}\left(\frac{r_s}{r_0} + \Lambda r_0^2\right)^2, \quad (30)$$

where β_1 is the expansion velocity (v/c) of the dust as seen by observers (who are stationary relative to the condensed mass) at the time the photon enters the Kottler hole, see Figure 1. Inserting this into Equation (22), we have the additional deflection angle α_{expand} caused by the extended trajectory of the photon in the Kottler void

$$\alpha_{\mathrm{expand}} = \left(\frac{r_s}{2r_0}\right)\cos\tilde{\phi}_1\Bigg[6\sin^2\tilde{\phi}_1 - 12\cos\tilde{\phi}_1 \times \sin\tilde{\phi}_1\sqrt{\frac{\Lambda r_0^2}{3} + \frac{r_s}{r_0}\sin^3\tilde{\phi}_1} + \Lambda r_0^2\left(\frac{8}{3} - \frac{20}{3}\sin^2\tilde{\phi}_1\right)\Bigg] + \left(\frac{r_s}{2r_0}\right)^2\Bigg[6\cos\tilde{\phi}_1(4\sin\tilde{\phi}_1 - \sin^2\tilde{\phi}_1 + 2\sin^3\tilde{\phi}_1 - 11\sin^5\tilde{\phi}_1) - 12\log\left\{\tan\frac{\tilde{\phi}_1}{2}\right\}\sin^3\tilde{\phi}_1\Bigg] + \mathcal{O}\left(\frac{r_s}{r_0} + \Lambda r_0^2\right)^{5/2}. \quad (31)$$

Combining Equations (23) and (31), we obtain the total bending angle α_{total} caused by a photon entering and exiting a Kottler condensation

$$\alpha_{\mathrm{total}} = \left(\frac{r_s}{2r_0}\right)\cos\tilde{\phi}_1\Bigg[-4\cos^2\tilde{\phi}_1 - 12\cos\tilde{\phi}_1 \times \sin\tilde{\phi}_1\sqrt{\frac{\Lambda r_0^2}{3} + \frac{r_s}{r_0}\sin^3\tilde{\phi}_1} + \Lambda r_0^2\left(\frac{8}{3} - \frac{20}{3}\sin^2\tilde{\phi}_1\right)\Bigg] + \left(\frac{r_s}{2r_0}\right)^2\Bigg[\frac{15}{4}(2\tilde{\phi}_1 - \pi) + \cos\tilde{\phi}_1\left(4 + \frac{33}{2}\sin\tilde{\phi}_1 - 4\sin^2\tilde{\phi}_1 + 19\sin^3\tilde{\phi}_1 - 64\sin^5\tilde{\phi}_1\right) - 12\log\left\{\tan\frac{\tilde{\phi}_1}{2}\right\}\sin^3\tilde{\phi}_1\Bigg] + \mathcal{O}\left(\frac{r_s}{r_0} + \Lambda r_0^2\right)^{5/2}. \quad (32)$$

The reader should observe that a negative contribution to the bending angle is toward the lens and a positive contribution is away from it. Also recall that these approximate expressions were derived assuming $\sin\tilde{\phi}_1 \gg r_s/r_0$. Our deflection angle accounts for the finite time (equivalently range) that gravity has to act on the passing photon as well as aberration effects caused by switching between moving observers. A finite range is equivalent to a shielding of the perturbation's mass by the

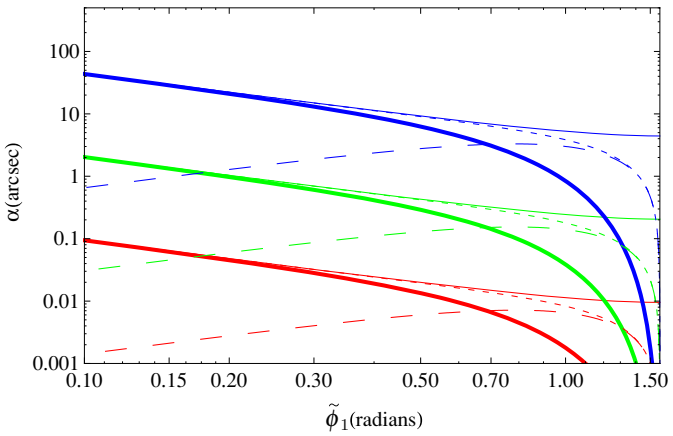

Figure 3. Three sets of the deflection angles α corresponding to three deflector masses $10^{11}\,M_\odot$ (lower in red), $10^{13}\,M_\odot$ (middle in green), and $10^{15}\,M_\odot$ (top in blue) at redshift $z = 1$ are shown as functions of the azimuthal angle $\tilde{\phi}_1$. The thick lines are $|\alpha_{\rm total}|$ of Equation (32), the short dashed lines are $|\alpha_{\rm static}|$ of Equation (23), the dashed lines are $\alpha_{\rm expand}$ of Equation (31), and the thin solid lines are the Einstein values $2r_s/r_0$. All deflection angles are toward the deflector except $\alpha_{\rm expand}$ which is away from the deflector, i.e., in this plot $|\alpha_{\rm total}| = |\alpha_{\rm static}| - \alpha_{\rm expand}$.

(A color version of this figure is available in the online journal.)

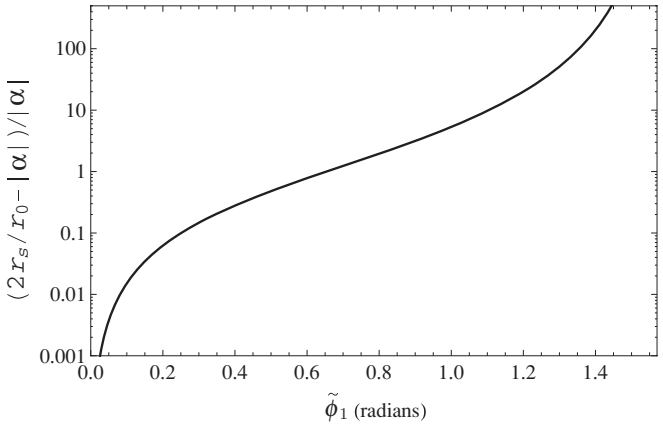

Figure 4. Fractional difference of the Einstein deflection angle $2r_s/r_0$ and $\alpha_{\rm total}$ given in Equation (32), i.e., $(2r_s/r_0 - |\alpha_{\rm total}|)/|\alpha_{\rm total}|$ as a function of $\tilde{\phi}_1$ in radians. For the domain of $\tilde{\phi}_1$ plotted and to the accuracy shown, the fractional error is remarkably independent of the mass of the deflector (10^{11}–$10^{15}\,M_\odot$) and its redshift ($0 < z < 2$).

homogeneous distribution of its neighbors; i.e., beyond r_b of Equation (7) the effect of the neighbors completely suppresses the effects of the inhomogeneity. The deflection angle $\alpha_{\rm total}$ appropriately vanishes in the limit $\tilde{\phi}_1 \to \pi/2$, i.e., when the photon only grazes the condensation, and for small $\tilde{\phi}_1$ the lowest order term in the bending angle approaches the Einstein value $4Gm/c^2r_0$ as expected. For an arbitrary impact $\tilde{\phi}_1$, however, the linear term in $\alpha_{\rm total}$ is

$$\alpha_{\rm linear} = -4\left(\frac{r_s}{2r_0}\right)\cos^3\tilde{\phi}_1, \tag{33}$$

and, in some weak-lensing circumstances, predicts potentially detectable differences from the Einstein value. In standard lensing calculations (see Bourassa & Kantowski 1975), there is no attempt to make the deflector's gravity field part of the cosmology's gravity field as GR really requires. Deflector masses are simply taken as additions to the cosmology's mean mass density and consequently have "∞" range. Swiss cheese, the only known and relevant GR solution, makes the deflector mass a contributor to the cosmology's mean density and as a consequence, the gravity field of the deflector is limited in range. This limited range is seen to be important when the impact angle is above a tenth of a radian (Figure 4).

Another somewhat surprising result is that the lowest order correction to the Einstein value, other than the finite time effect represented by the dependence on $\tilde{\phi}_1$, is the dependence on the expansion rate, i.e., the square root term in Equations (31) and (32) (see Equation (16)). We can interpret the source of this term as the extra time (or equivalently distance) the Schwarzschild mass has to act on the passing photon. The Kottler hole expands in size as the photon traverses, and since the cosmological constant contributes to the Hubble expansion, it contributes to the extra time. Others have also argued that Λ affects α, e.g., Sereno (2009) finds a Λ contribution to small angle bending of order $(r_s/r_0)\Lambda r_0^2$ which we do find even if of opposite sign and differing amount, Ishak (2008) and Ishak et al. (2008) find a term of order $\Lambda r_0 r_b \sim \Lambda r_0^2 \csc\tilde{\phi}_1$, which we do not. The most important Λ correction that we find, i.e., the square root term in Equation (32), seems to have gone undetected by others because of the approximations they used. In the next section, we estimate just how important these corrections to the Einstein result can be.

4. DISCUSSION

In Figure 3, we have plotted three sets of bending angles for three deflecting masses ranging from a large galaxy mass to a rich cluster mass, respectively $10^{11}\,M_\odot$ (lower in red), $10^{13}\,M_\odot$ (middle in green), and $10^{15}\,M_\odot$ (top in blue) all at redshift $z = 1$. Note that redshift z plays a part because redshift influences the entrance/exit size of the Kottler hole, see Equations (5) and (7). The cosmological parameters we used are $\Omega_m = 0.3$, $\Omega_\Lambda = 0.7$, and $H_0 = 70\,{\rm km\,s^{-1}Mpc^{-1}}$. For each mass, we have plotted four bending angles in arcseconds as functions of $\tilde{\phi}_1$ (the supplement of the azimuthal impact angle). The thick lines are $|\alpha_{\rm total}|$ of Equation (32), the short dashed lines are $|\alpha_{\rm static}|$ of Equation (23), the dashed lines are $\alpha_{\rm expand}$ of Equation (31), and the thin solid lines are the Einstein values $2r_s/r_0$. All deflection angles are negative (attractive), i.e., toward the deflector, except $\alpha_{\rm expand}$, which is away from the deflector. Because of the log–log scale, it was necessary to plot absolute magnitudes, i.e., $|\alpha_{\rm total}| = |\alpha_{\rm static}| - \alpha_{\rm expand}$. The reader can easily see (to the accuracy of the plot) that if $\alpha_{\rm expand}$ is neglected the deflection angle follows $2r_s/r_0$ out to $\sim 30^\circ$, however, when $\alpha_{\rm expand}$ is included the deflection angle follows $2r_s/r_0$ only out to $\sim 10^\circ$. This observation is clearly independent of the masses shown and in fact is quite independent of the deflectors' redshifts. The fractional difference in $\alpha_{\rm total}$ and the Einstein value plotted in Figure 4 is independent of the deflector's mass (10^{11}–$10^{15}\,M_\odot$) and redshift ($0 < z < 2$) for the range of $\tilde{\phi}_1$ plotted. Noticeable redshift-dependent differences would begin to appear for the three masses only below $\tilde{\phi}_1 \sim 2^\circ$. From Figure 4, we can conclude that for angles above $\sim 4^\circ$ the fractional differences of $\alpha_{\rm expand}$ and the Einstein values are greater than 1% and above $\sim 40^\circ$ the differences are above 100%.

In Table 1, we use our corrected bending angle Equation (32) to estimate corrections in bending angles for strong and weak lensing by clusters and elliptical galaxies. We look at the following cases: the large image separation cluster lens A1689 at $z = 0.18$, the high redshift cluster RDCS 1252−2927 at $z = 1.24$, and a typical $z = 0.5$ elliptical galaxy. In A1689, we calculate the bending angle corrections for the largest arc

separation of 45″ for strong- and weak-lensing measurements at 10′ away from center (Umetsu & Broadhurst 2008) by using the mass profile of recent X-ray measurements (Peng et al. 2009). We also calculate the correction in a high redshift cluster RDCS 1252−2927, where the weak-lensing signals have been detected out to 3′ (Lombardi et al. 2005). For lensing by galaxies, we choose a typical elliptical galaxy at $z = 0.5$ and use the mass profile and weak-lensing detections in Gavazzi et al. (2007). In general, we find that the corrections in the bending angles for strong lensing are quite small; e.g., the largest correction $(1 - \cos^3 \tilde{\phi}_1)$ is just 0.07% for the largest separated arcs in A1689. However, for weak lensing, the correction can reach 2% for the weak-lensing signals detected in the outermost regions of the cluster in A1689, and the correction can reach 5% for the $z = 1.24$ cluster RDCS 1252−2927. For the weak-lensing signals detected using an ensemble of elliptical galaxies (Gavazzi et al. 2007), the correction is 4% for the outermost bin. A correction of this amount will present an additional challenge for using weak lensing as a tool for precision cosmology. For the corrections involving the Λ term, the largest is 0.02% for weak lensing in high redshift clusters, which is not detectable in current observations. We expect our model to be relevant for weak lensing induced by the large-scale structure including weak lensing of the cosmic microwave background, where even larger volumes are involved. We expect a large correction due to the $1 - \cos^3 \tilde{\phi}_1$ term and a presumably detectable correction involving Λ.

The corrections we give for strong lensing are negligible because $\tilde{\phi}_1$ is small and only a small fraction of the inhomogeneous mass appears inside the Einstein ring. For these cases, our corrections may not be accurate because the effective lensing mass is not spherically distributed as it is in our model. Nonlinear corrections are conceivably sensitive to the difference in cylindrical and spherical symmetry. More realistic models are needed to fully constrain corrections for strong lensing. In general, the applicability of the corrected deflection angle $\alpha_{\rm total}$ in Equation (32) is limited to spherical inhomogeneities, the majority of whose mass is within the minimum impact of the light ray. This is because we used a fully condensed Swiss cheese model; i.e., the homogeneity is represented by a Schwarzschild mass. Because we are calculating nonlinear corrections, one cannot expect Equation (32) to give an accurate answer by simply including that fraction of the mass within the impact cylinder as is normally done in lensing. Consequently, more accurate mass profiles in the Swiss cheese would be appropriate for the strong-lensing examples in Table 1.

Work on this paper was initiated to correctly quantify the cosmological constant's effect on small angle deflections of photons caused by mass inhomogeneities in an otherwise homogeneous cosmology. By using an exact solution to GR, we established that Λ's effect is nonlinear thus requiring use of a gravity theory beyond Newton's. The model we used, a flat Swiss cheese cosmology, also predicts a significant decrease in the deflection angle caused by the shielding of an inhomogeneity by its homogeneously distributed neighbors. Shielding occurs because the deflectors are contributors to the cosmology's mean density. Standard lensing calculations completely overlook shielding because deflectors are treated as additions to the mean.

Perturbations to $\alpha_{\rm total}$ would obviously exist if the neighbors generated a shear at the site of the deflector. The accuracy of Swiss cheese predictions depends on the scale at which inhomogeneous matter follows the background Hubble flow, i.e., on what scale the cosmological principle is satisfied. The simple Swiss cheese model used here does not allow for peculiar motions but does account for the scale of the cosmology affected by an inhomogeneity; i.e., beyond r_b the perturbed spacetime returns to the mean cosmic flow. In the neighborhood of the Local Group, where good observational data are available, most galaxies follow the Hubble flow with only small deviations (e.g., Karachentsev et al. 2009). A hierarchical Swiss cheese condensation could be used to include shear and peculiar motion but it would not only complicate this calculation by introducing several additional parameters, it would most certainly obscure the source of the Λ term in the results. To keep the result as simple as possible, we did not attempt to estimate the size of these additional perturbations.

Our results, e.g., Equation (32), are stated in terms of the parameters $\tilde{\phi}_1$ and r_0 described in Section 3 and Figure 1 and are not necessarily the most convenient ones to use in lensing applications, however, they were convenient for the above derivations. To have the incoming photon travel parallel to the x-axis, one only has to rotate the coordinates clockwise an amount ξ_1 given in Equation (14).

This work was supported in part by NSF grant AST-0707704 and US DOE Grant DE-FG02-07ER41517. B.C. also thanks the University of Oklahoma Foundation for a fellowship.

REFERENCES

Bertotti, B. 1966, Proc. R. Soc. A, 294, 195
Bondi, H. 1947, MNRAS, 107, 410
Bourassa, R. R., & Kantowski, R. 1975, ApJ, 195, 13
Dashevskii, V. M., & Slysh, V. I. 1966, Sov. Astron., 9, 671
Dashevskii, V. M., & Zel'dovich, Ya. B. 1965, SvA, 8, 854
Dyer, C. C., & Roeder, R. C. 1974, ApJ, 189, 167
Einstein, A., & Straus, E. G. 1945, Rev. Mod. Phys., 17, 120
Gavazzi, R., Treu, T., Rhodes, J. D., Koopmans, L. V. E., Bolton, A. S., Burles, S., Massey, R. J., & Moustakas, L. A. 2007, ApJ, 667, 176
Gunn, J. E. 1967, ApJ, 150, 737
Ishak, M. 2008, Phys. Rev. D, 78, 103006
Ishak, M., Rindler, W., & Dossett, J. 2010, MNRAS, 403, 2152
Ishak, M., Rindler, W., Dossett, J., Moldenhauer, J., & Allison, C. 2008, MNRAS, 388, 1279
Kantowski, R. 1969a, ApJ, 155, 89
Kantowski, R. 1969b, ApJ, 155, 1023
Kantowski, R., Vaughan, T., & Branch, D. 1995, ApJ, 447, 35
Karachentsev, I. D., Kashibadze, O. G., Makarov, D. I., & Tully, R. B. 2009, MNRAS, 393, 1265
Khriplovich, I. B., & Pomeransky, A. A. 2008, Int. J. Mod. Phys. D, 17, 2255
Kottler, F. 1918, Ann. Phys., Lpz., 361, 401
Lemaître, G. 1933, Ann. Soc. Sci. Brux., A53, 51
Lombardi, M., et al. 2005, ApJ, 623, 42
Park, M. 2008, Phys. Rev. D, 78, 023014
Peng, E.-H., Andersson, K., Bautz, M. W., & Garmire, G. P. 2009, ApJ, 701, 1283
Rindler, W., & Ishak, M. 2007, Phys. Rev. D, 76, 043006
Schücker, T. 2009a, Gen. Rel. Grav., 41, 67
Schücker, T. 2009b, Gen. Rel. Grav., 41, 1595
Schücking, E. 1954, Z. Phys., 137, 595
Sereno, M. 2008, Phys. Rev. D, 77, 043004
Sereno, M. 2009, Phys. Rev. Lett., 102, 021301
Tolman, R. C. 1934, Proc. Natl Acad. Sci. USA, 20, 169
Umetsu, K., & Broadhurst, T. 2008, ApJ, 684, 177
Zel'dovich, Ya. B. 1964, Sov. Astron., 8, 13